Superconductor Science and Technology

PAPER

# Artificial pinning centers in $MgB_2$ superconducting bulks



IOP Publishing Superconductor Science and Technology
Supercond. Sci. Technol. 33 (2020) 045013 (7pp) https://doi.org/10.1088/1361-6668/ab7471

# Artificial pinning centers in $MgB_2$ superconducting bulks

**L B S Da Silva[1,4], A Serquis[2], E E Hellstrom[3] and D Rodrigues Jr[1]**

[1] Escola de Engenharia de Lorena, Universidade de São Paulo, Lorena, SP, Brazil
[2] Centro Atomico Bariloche, INN-CONICET-CNEA, San Carlos de Bariloche, RN, Argentina
[3] Applied Superconductivity Center, Florida State University, Tallahassee, FL, United States of America

E-mail: lucasarno@usp.br and durval@demar.eel.usp.br

Received 12 November 2019, revised 31 January 2020
Accepted for publication 10 February 2020
Published 28 February 2020

**Abstract**

The optimization of $MgB_2$ superconducting properties is extremely important for practical application. The introduction of an effective artificial pinning center in this material can enhance its critical current density efficiently. In this paper, $VB_2$ is described as a material that provides effective pinning in the $MgB_2$ bulks. The simultaneous addition of SiC as a carbon source is also analyzed. The samples were prepared using ball milling under a controlled atmosphere and heat treatment with a continuous argon flux. As a result, the superconducting properties could be optimized due to the effective improvement in the pinning behavior as well as with the carbon doping.

Keywords: $MgB_2$, artificial pinning center, $VB_2$, addition, SiC doping, critical current density, pinning

(Some figures may appear in colour only in the online journal)

## 1. Introduction

$MgB_2$, with its known superconductivity since 2001 [1], is considered a strategic material for practical applications. The principal characteristics of this superconducting material are the high value of its critical temperature (~39 K), the transport capacity (~$10^6$ A cm$^{-2}$) and the absence of weak-link problems [2]. Another advantage of this material is the possibility to improve its superconducting properties through small changes in the synthesis parameters. The principal mechanisms that can be optimized through the synthesis process are the grain connectivity, densification, MgO growth, pinning, and doping.

Many research groups have worked with chemical doping in an attempt to replace Mg and/or B in the crystalline structure of $MgB_2$. Some chemical elements, such as Ti, Zr, Hf, Al, Mn, Li, Si, Ta, Zr and others [3–9], were used as doping elements. Changes in the intrinsic properties were observed, such as the enhancement of the critical temperature ($T_c$) and the upper critical magnetic field ($H_{c2}$). Other effective doping methods occur with addition of carbon sources (including organic sources) [9–16], causing the replacement of B with C atoms in the crystalline structural of $MgB_2$ [10, 11].

Another procedure which has been used to improve the critical current density is the addition of structural defects in the $MgB_2$ matrix. These defects can act as efficient pinning centers if their dimensions are comparable to the coherence length of $MgB_2$ [12]. In recent years, the Group of Superconductivity of the Lorena Engineering School—University of São Paulo, in collaboration with other groups, have worked with addition of other diborides in the $MgB_2$ phase. These diborides, with the same $AlB_2$ crystalline structure as $MgB_2$ [7–9, 15, 17, 18], proved to be a good option for pinning improvement. In previous works using $TaB_2$ and $ZrB_2$ as additions [7–9] it could be seen that the critical current density of the material was enhanced. That behavior was attributed to the fact that Ta and Zr doping can replace Mg atoms in the crystalline structure of $MgB_2$ and simultaneously improveme pinning with the introduction of defects in the superconducting matrix. The addition of $AlB_2$ and $VB_2$ was also tested previously [15], and the effect of this new composite in the $MgB_2$ superconducting properties is also the enhancement of the critical current density. However, the reasons for this improvement were unknown. The enhancements in the $MgB_2$ superconducting properties when other diboride are added in the production process of $MgB_2$ is the main motivation to continue studying this method. $VB_2$ is specially interesting

[4] Author to whom any correspondence should be addressed.

 

**Table 1.** Powders specification.

| Powders | Specification |
|---|---|
| Mg | AlfaAesar, –325 mesh, 99.8% |
| B | AlfaAesar, –325 mesh, 99% |
| $VB_2$ | CERAC, –325 mesh, 99.5% |
| SiC | AlfaAesar, 20–30 nm, 97.0% |

**Table 2.** Stoichiometry and sample names for $MgB_2$ bulks.

| Sample parameters | Sample names |
|---|---|
| Pure $MgB_2$ | $MgB_2$ pure |
| $MgB_2$ + 10 wt% SiC | $MgB_2$ + SiC |
| $MgB_2$ + 2 at% $VB_2$ | $MgB_2$ + 2% $VB_2$ |
| $MgB_2$ + 2 at% $VB_2$ + 10 wt% SiC | $MgB_2$ + 2% $VB_2$ + SiC |

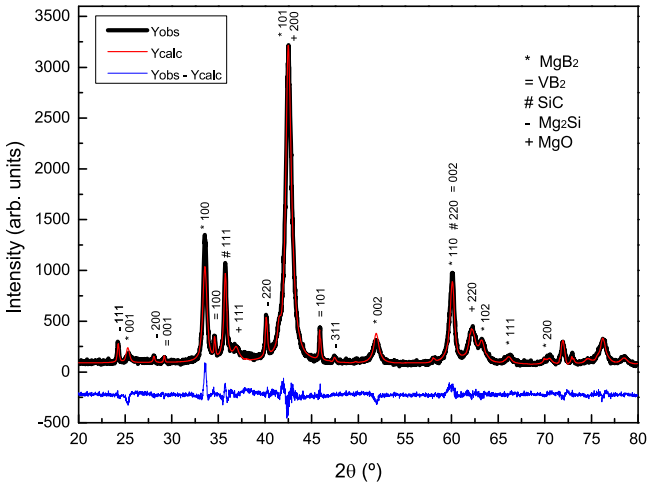


**Figure 1.** X-ray difractogram refinement for the $MgB_2$ + 2% $VB_2$ + SiC.

due the immiscibility between V and Mg, with the possibility to study only the effect of the introduction of artificial pinning centers in the superconducting properties of $MgB_2$ without doping.

In this work, $VB_2$ is mixed with $MgB_2$ during the preparation process, using ball milling and a controlled atmosphere. Samples with simultaneous additions of $VB_2$ and SiC were also prepared, focusing on the improvement of critical current density and irreversible magnetic field, important characteristics for practical applications. A detailed discussion is made in an attempt to define the influence of this addition on the $MgB_2$ superconducting behavior and on the pinning mechanisms acting in the material. The microstructural and crystallographic characterization were simultaneously analyzed alongside the superconducting properties.

## 2. Experimental procedure

$MgB_2$ superconducting bulks with the addition of $VB_2$ and simultaneous addition of $VB_2$ and SiC were prepared. The use of $VB_2$ is an attempt to introduce artificial pinning centers in the superconducting matrix. SiC is a carbon source to enhance the irreversibility field [10, 11]. The production methodology uses the *in situ* method, ball milling under nitrogen atmosphere and heat treatment with continuous argon flux.

Table 1 shows the specification of the initial material. Pure powders of Mg and B and powders with 2 at% of $VB_2$ and with 10 wt% of SiC were mixed using a ball mill machine (Fritsch—Laborgerätebau, Industriests 8) for 1 h in a glovebox with controlled atmosphere of nitrogen. The powders were compacted using a uniaxial press under a pressure of ∼10 MPa. The heat treatment was performed under continuous argon flux and with a 5 °C $min^{-1}$ heating rate to 600 °C, holding for 2 h, and slow cooling with a 2 °C $min^{-1}$ rate to room temperature. This profile of heat treatment was chosen to promote the sintering, densification and improvement of the intergrain connectivity [7, 19, 20]. Table 2 shows the $MgB_2$ samples prepared and analyzed in this work.

The crystallographic characterization was performed with a Shimadzu model XRD 6000 diffractometer at room temperature, using Ni-filtered Cu-K$\alpha$ x-ray radiation (1.5417 Å), scanning between 20° and 80° and with an angular step of 0.02° in 2$\theta$ with 1 s of counting per point. The samples were measured as powders, to avoid preferred orientations. The crystallographic refinement was simulated using the Full Prof software (freeware), and the Rietveld method [21].

Microstructural characterization was performed using a scanning electron microscope (SEM, model LEO 1450VP) with an Oxford energy dispersive spectrometer (EDS), and JEOL JEM 2100 $LaB_6$ transmission electron microscopy (TEM) with a Thermo-Noran EDS.

Optical characterization was performed using a Micro-Raman spectrometer (Renishaw 2000T 64000), with 747 nm light radiation and *xy* polarization. Polarization was used to analyze only the $E_{2g}$ phonon radiation, due to the strong electron-phonon interactions.

A Quantum Design Evercool II physical properties measurement system (PPMS) with vibration sample measurement (VSM) was used to perform the superconducting characterization and extract the superconducting parameters.

## 3. Results and discussion

A compilation of the x-ray crystallography characterization and crystalline refinement using the Rietveld method is showed in table 3. Figure 1 displays the x-ray diffractogram after refinement for the sample of $MgB_2$ with simultaneous addition of 2 at% of $VB_2$ and 10 wt% of SiC. The $Y_{obs}$—$Y_{calc}$ curve and the value of $chi^2$, demonstrate the good quality of the refinement.

For all samples the presence of MgO was detected, with values ranging between 15 and 20 wt% even with all experimental care taken during the preparation process of the bulks. This behavior is intrinsic of the production process, when working with Mg and B, due to the easy oxidation of these elements. The grown of $Mg_2Si$ is due to the SiC addition and

**Table 3.** Summary of the structural phase refinement for the $MgB_2$ samples.

| Samples | $MgB_2$ (wt%) | $VB_2$ (wt%) | SiC (wt%) | MgO (wt%) | $Mg_2Si$ (wt%) | $MgB_2$ | | chi$^2$ |
|---|---|---|---|---|---|---|---|---|
| | | | | | | *a* (Å) | *c* (Å) | |
| $MgB_2$ pure | 83.0 | — | — | 17.0 | — | 3.086(1) | 3.523(1) | 1.57 |
| $MgB_2$ + SiC | 72.1 | — | 10.1 | 15.0 | 2.8 | 3.084(1) | 3.523(1) | 1.83 |
| $MgB_2$ + 2% $VB_2$ | 83.7 | 1.4 | — | 14.8 | — | 3.084(1) | 3.521(1) | 2.44 |
| $MgB_2$ + 2% $VB_2$ + SiC | 77.1 | 0.8 | 2.7 | 19.1 | 0.4 | 3.084(1) | 3.522(1) | 2.69 |

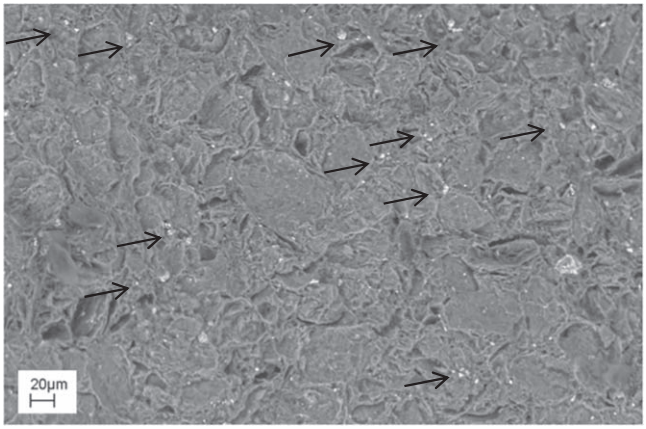


**Figure 2.** $MgB_2$ + $VB_2$ microstructure using backscattered electrons detection mode. The arrows indicate some $VB_2$ grains.

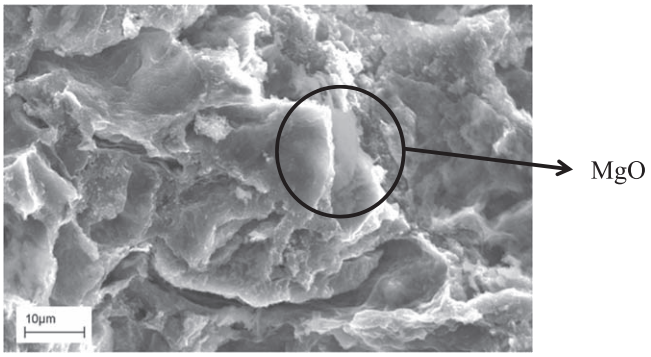


**Figure 3.** $MgB_2$ + $VB_2$ microstructure using secondary electrons detection mode.

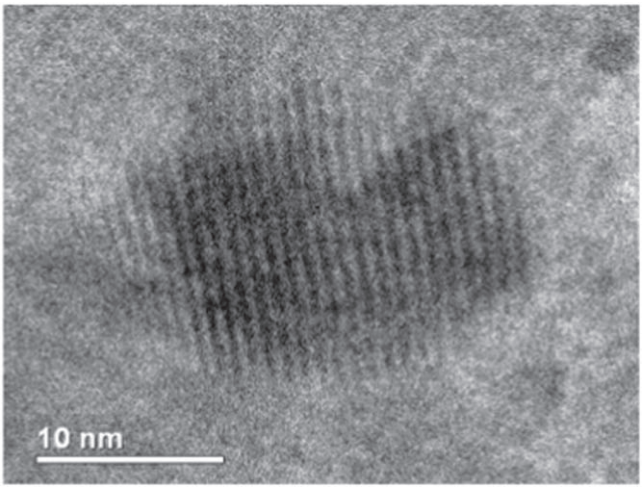


**Figure 4.** $MgB_2$ + $VB_2$ microstructure using TEM. In the center of the picture one $VB_2$ grain is shown, with a 101 orientation.

an evidence for C doping. Even with Mg oxidation and the addition of new elements, the $MgB_2$ phase is between 72 and 83 wt% of the total bulk. The XRD analysis corresponds to a small fraction of the total bulk, and the SiC concentration in the $MgB_2$ + 2% $VB_2$ + SiC sample shows that the SiC phase may be more concentrated in certain bulk regions and not homogeneously distributed in the $MgB_2$ matrix.

Using conventional XRD, the lattice parameters *a* and *c* do not present significant changes. However, it is known that even a small amount of a C source is enough to promote C doping in the $MgB_2$ crystalline structure [22]. Maybe a more accurate technique can identify some significant changes in the $MgB_2$ lattice parameter. On the other hand, as expected due to the immiscibility between Mg and V, the lattice parameter *a* and *c* also do not present significant changes, when $VB_2$ is added.

Figure 2 shows the microstructure of the $MgB_2$ matrix with addition of $VB_2$ powders, using the backscattered electron detection mode and fractured sample. Some small grains of $VB_2$ randomly scattered in the $MgB_2$ matrix can be identified by the contrast difference. High densification and a lack of pores in the superconducting matrix is observed, important characteristics for superconducting properties.

Figure 3 displays the microstructure of the $MgB_2$ + $VB_2$ sample, using a secondary electron detecting mode and fractured sample. The MgO phase is seen as a thin cloud around the $MgB_2$ matrix. The amount of these oxide regions could be quantified with x-ray diffractometry analyses (∼15–20 wt%). These MgO in excess can be prejudicial to the superconducting properties because they affect the inter-grain connectivity [23].

Figure 4 exhibits the microstructure of a $VB_2$ grain, analyzed using TEM in high-resolution mode. This micrograph shows the 101 orientation, with an interplanar distance of ∼1 nm. A diameter of about 15 nm was estimated treating this grain as a sphere. The size of these inclusions is important for the effective performance as artificial pinning centers, improving the $J_c$ and $H_{irr}$ of the samples. The $VB_2$ grain is embedded in the $MgB_2$ superconducting matrix.

Figure 5 presents the $E_{2g}$ Raman phonon spectroscopy for all samples, with *xy* polarization. All curves follow the same behavior and the peaks of the maximum for the $E_{2g}$ Raman phonon show a thin dislocation to higher energy when SiC and $VB_2$ are added in the production process, compared with the

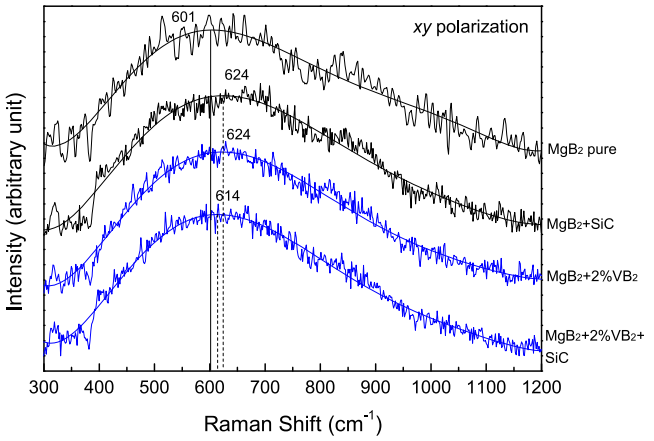


**Figure 5.** $E_{2g}$ Raman phonon spectroscopy with *xy* polarization.

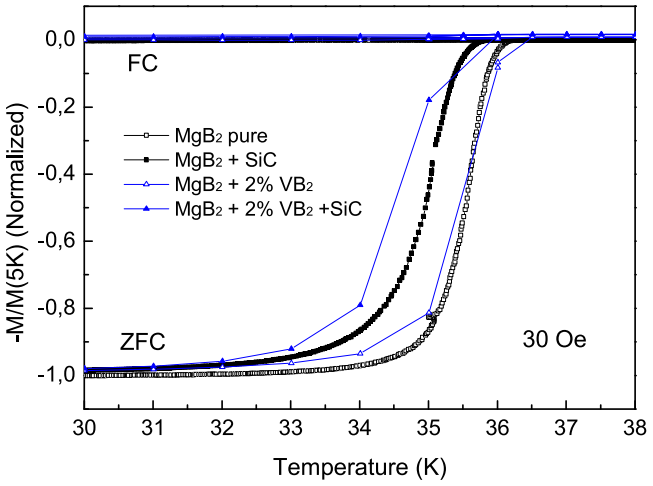


**Figure 6.** Normalized magnetization as a function of temperature, under an applied magnetic field of 30 Oe.

pure $MgB_2$ sample. According to Parisiades *et al* 2009 [22], $MgB_2$ doping with different materials could displace the peak maximum. This displacement to high energy can be caused by C doping with the replacement of B to C atoms in the $MgB_2$ crystalline structure. The dislocation of about 23 $cm^{-1}$ in the peak maximum of $E_{2g}$ Raman phonon for samples with the addition of SiC is evidence of $MgB_2$ C-doping. On the other hand, as V is immiscible with Mg, the dislocation of the $E_{2g}$ peak maximum may be explained by the disorder caused by $VB_2$ inclusions in the superconducting matrix.

Figure 6 illustrates the curves of normalized magnetization as a function of temperature in the regimes of zero field cooled (ZFC) and field cooled (FC). The critical temperatures by magnetization could be extracted as the intersection point between ZFC and FC. The values of $T_{cMAG}$ are detailed in table 4. The addition of $VB_2$ does not lead to a significant change in $T_{cMAG}$, which means that the $VB_2$ was not incorporated in the superconducting matrix as a dopant. The sharp shape of the superconducting-normal transition and the small values of $\Delta T_c$ express the good homogenization of the superconducting phase.

The $T_{cMAG}$ values decrease for samples with the addition of SiC, compared with the pure $MgB_2$ sample. This behavior is clear evidence of the carbon doping and it is in agreement with the Raman spectrum. According to Dou *et al* 2002 [10], the C atoms replace the B atoms in the crystalline structure of $MgB_2$.

Still using the magnetic hysteresis curves in the ZFC and FC regimes, the magnetic susceptibility as a function of temperature was used to estimate the superconducting fraction. The demagnetization factor due to the parallelepiped geometry of the sample was considered and was estimated according to Sato, 1989 [24]. The values of superconducting fraction can be seen in table 4. These values show the large amount of impurities and unreacted $MgB_2$ phase.

DC magnetization loops versus applied magnetic field at 5 K and 20 K were used to extract the $J_c$ (H, T = 5 K and 20 K) versus $\mu_0 H$ curves using

$$J_c = \frac{20\Delta M}{a_1\left(1 - \frac{a_1}{3a_2}\right)} \quad (1)$$

where $\Delta M$ is the difference of magnetization in a given field, $a_1$ and $a_2$ ($a_1 < a_2$) are the lengths of the parallelepiped edges perpendicular to the magnetic field, and $J_c$ is given in CGS units. This equation follows the Bean critical model [25]. Table 4 also presents the irreversibility fields $H_{irr}$ and upper critical field $H_{c2}$ determined using the onset of $M$ versus $\mu_0 H$ curves and the intersection of $M$ versus $\mu_0 H$ curve with the abscissa axis, respectively. Figure 7(a) is an example how the $H_{irr}$ and $H_{c2}$ were determined, according to Fuchs *et al* [26] criterion. For the samples measured at 5 K, the $H_{irr}$ and $H_{c2}$ are higher than the applied magnetic field, therefore the $M$ versus $\mu_0 H$ curves were fitted and extrapolated to estimate the $H_{irr}$ (figure 7(b)), $H_{c2}$ could not be found.

Figure 8 shows the curves of critical current densities as a function of the applied magnetic field, at 5 K and 20 K. Under high magnetic field, the values of $J_c$ for the samples with addition of SiC are higher than those obtained for the pure $MgB_2$ sample, due to carbon doping and the replacement of B with C atoms in the crystalline structure of $MgB_2$. However, the improvement of the critical current densities under high magnetic field for samples with addition of $VB_2$ has a different explanation. The addition of $VB_2$ in the superconducting matrix introduces crystalline defects in the material with sizes comparable to the coherence length of the $MgB_2$ (table 4), acting as efficient pinning centers. The enhancement in the value of $H_{irr}$ is another effect caused by the same reason. The reason for the enhancement of $J_c$ for the samples with $VB_2$ addition only under a high magnetic field is exactly due to the action of artificial pinning centers addition, when the magnetic flux lines penetration is more intense.

When the sample is prepared with the combined addition of SiC and $VB_2$ the result is the enhancement of the critical current densities in high magnetic field and an effective improvement in the $MgB_2$ superconducting properties. The SiC addition acts as an effective carbon dopant and the $VB_2$ acts as effective pinning centers.

Figure 9 displays the curves of the pinning forces as a function of applied magnetic field. The inset of figure 9 exhibits the normalized curves of reduced flux pinning force $f_p = F_p/F_{pmax}$ as a function of reduced magnetic field $b = B/B_{c2}$ for all samples. The shape of the $f_p$ versus $b$ curves

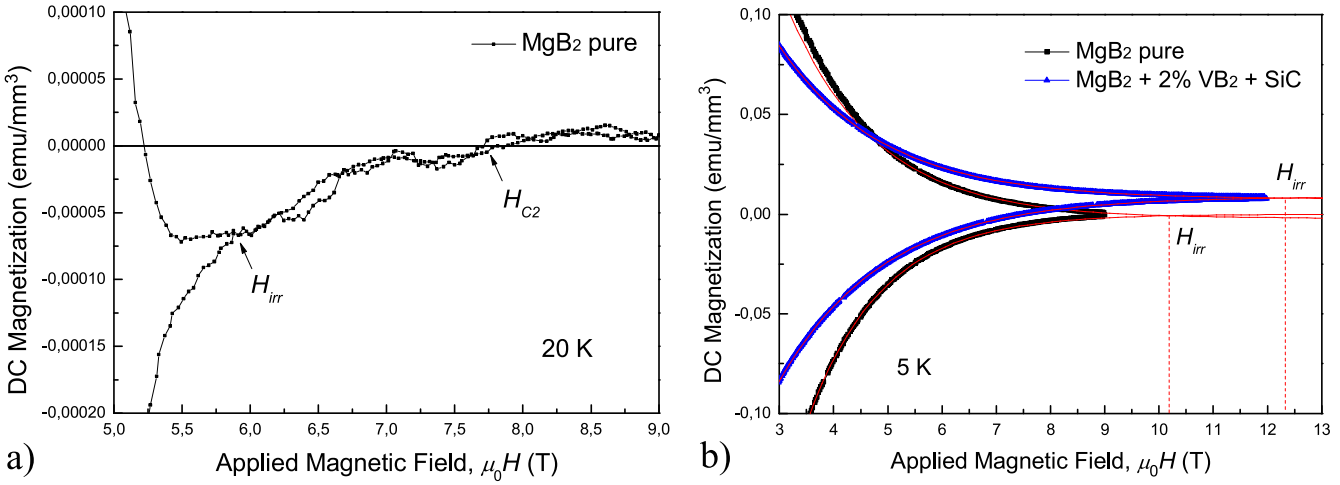


**Figure 7.** (a) Criterion used to determine the $H_{irr}$ and $H_{c2}$ at 20 K, according to Fuchs *et al* [26], and (b) fitting and extrapolation of $M$ versus $\mu_0 H$ curve to estimate the $H_{irr}$ at 5 K.

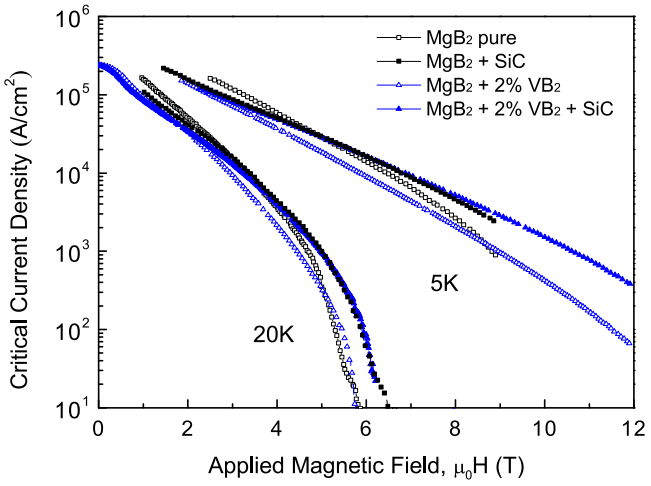


**Figure 8.** Critical current density as a function of applied magnetic field, at 5 K and 20 K.

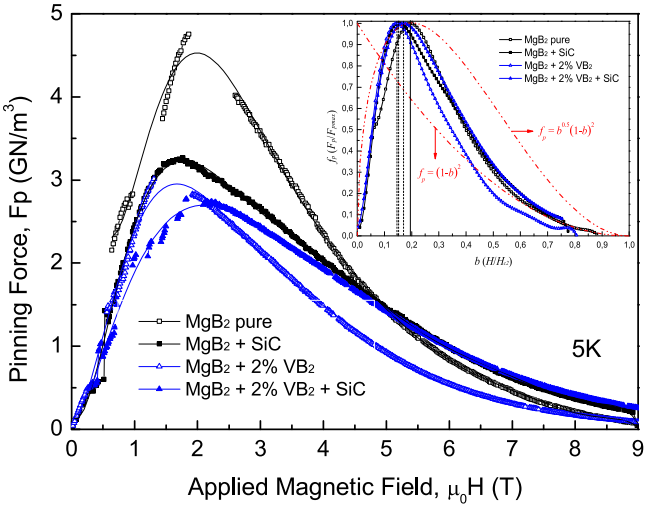


**Figure 9.** Pinning force as a function of applied magnetic field at 5 K. The inset displays the reduced flux pinning force as a function of reduced field.

indicates the pinning mechanisms acting in the sample, according to the Dew-Hughes model [27, 28]. As expected, due to the granular nature of the $MgB_2$ superconducting phase, the pinning mechanism acting in the pure sample is essentially due to the grain-boundaries (nucleon-surface-normal, $f(b) = b^{0.5}(1-b)^2$, reduced magnetic field when $f_p$ is maximum $b_{f_{pmax}} = 0.2$). Under a high magnetic field the pinning forces of the samples with the addition of $VB_2$ are higher than those observed for the others. The addition of SiC is another way to improve the pinning forces. The addition of SiC also changes the shape of the $f_p$ versus $b$ curves and it shifts the $b_{f_{pmax}}$ to lower values (table 4), an indication that another pinning mechanism is acting simultaneously with the grain-boundaries pinning, probably due to a normal phase (nucleon-volume-normal, $f(b) = (1-b)^2$). These normal phases can be the $VB_2$, unreacted SiC and/or $Mg_2Si$, according to the XRD analyzes.

Table 4 presents the values of the coherence lengths for samples at 20 K. The average coherence length is around 7 nm at 20 K, comparable to the grain size of the $VB_2$ included in the superconducting matrix (figure 4). These sizes of the coherence length and the superconducting behavior are clear evidence that the addition of $VB_2$ in the preparation process was efficient, producing effective pinning, which agrees with the $F_p$ versus $\mu_0 H$ and $f_p$ versus $b$ curves (figure 9).

The coherence lengths were calculated using the following equation

$$\xi(T) = \sqrt{\frac{\phi_0}{2\pi H_{c2}(T)}} \qquad (2)$$

where, $\phi_0 = \dfrac{h}{2\pi} = 2.0679.10^{-15}\,\mathrm{Tm}^2$ is the magnetic flux quantum [26]. The values of $H_{c2}(T)$ were extracted at the intersection of $M$ versus $\mu_0 H$ curve with the abscissa axis [26].

**Table 4.** Superconducting parameters of the samples.

| Sample | $T_{cMAG}$ (K) | $\Delta T_c$ (K) | $H_{irr}$(5 K) (T) | $H_{irr}$(20 K) (T) | $H_{c2}$(20 K) (T) | $\xi$(20 K) (nm) | $b_{f_{pmax}}$ | Superc. Fraction |
|---|---|---|---|---|---|---|---|---|
| $MgB_2$ pure | 36.3 | 0.5 | ~10.2 | 5.9 | 7.7 | 7.5 | ~0.20 | 53% |
| $MgB_2$ + SiC | 35.9 | 0.9 | ~11.6 | 7.1 | — | — | ~0.15 | 76% |
| $MgB_2$ + 2%$VB_2$ | 36.5 | 0.8 | ~11.6 | 5.8 | 7.9 | 6.5 | ~0.14 | 63% |
| $MgB_2$ + 2%$VB_2$ + SiC | 36.0 | 1.1 | ~12.4 | 6.3 | 7.9 | 6.5 | ~0.17 | 68% |

## 4. Conclusion

The $MgB_2$ sample preparation methodology and the $VB_2$ and SiC additions were efficient, adding effective artificial pinning centers and effective doping, respectively improving the critical current densities of the material in a high magnetic field and enhancing the $H_{irr}$. With the combination of crystallography, microstructural, optical, and superconducting analyses it could be concluded that the reason for this enhancement in the superconducting properties of the samples could be attributed to carbon doping with the addition of SiC and to the introduction of $VB_2$ clusters acting as effective pinning centers. The sample that presents the best superconducting behavior is the $MgB_2$ with the simultaneous addition of 10 wt% of SiC and 2 at% of $VB_2$.

## Acknowledgments

The authors acknowledge the LME/LNNano, Brazil, for technical support during the electron microscopy work, and the financial support by São Paulo Research Foundation (FAPESP, grant #2018/11521-5), CNPq, and CAPES, Brazil and ANPCyT, Argentina. DRJ is a CNPq researcher and AS is CONICET-CNEA researcher.

## ORCID iDs

L B S Da Silva https://orcid.org/0000-0002-8086-0857
A Serquis https://orcid.org/0000-0003-1499-4782
E E Hellstrom https://orcid.org/0000-0001-8263-8662
D Rodrigues Jr https://orcid.org/0000-0001-6522-1777

## References

[1] Nagamatsu J, Nakagawa N, Muranaka T, Zenitani Y and Akimitsu J 2001 Superconductivity at 39 K in magnesium diboride *Nature* **410** 63
[2] Serquis A, Serrano G, Moreno S M, Civale L, Maiorov B, Balakirev F and Jaime M 2007 Correlated enhancement of $H_{c2}$ and *Jc* in carbon nanotube doped $MgB_2$ *Supercond. Sci. Technol.* **20** L12–5
[3] Feng Y, Zhao Y, Pradhan A K, Cheng C H, Yau J K F, Zhou L, Koshinzuka N and Murakami M 2002 Enhanced flux pinning in Zr-doped $MgB_2$ bulk superconductors prepared at ambient pressure *J. Appl. Phys.* **92** 2614
[4] Goto D, Machi T, Zhao Y, Koshizuka N, Murakami M and Arai S 2003 Improvement of critical current density in $MgB_2$ by Ti, Zr, and Hf doping *Physica. C* **392–396** 272–5
[5] Slusky J S *et al* 2001 Loss of superconductivity with the addition of Al to $MgB_2$ and a structural transition in $Mg_{1-x}Al_xB_2$ *Nature* **410** 343
[6] Parisiades P, Liarokapis E, Zhigadlo N D, Katrych S and Karpinski J 2009 Raman Investigations of C, Li and Mn doped $MgB_2$ *J. Supercond. Nov. Magn.* **22** 169–72
[7] Da Silva L B S, Serrano G, Serquis A, Metzner V C V and Rodrigues D Jr 2015 Study of $TaB_2$ and SiC additions on the properties of $MgB_2$ superconducting bulks *Supercond. Sci. Technol.* **28** 025008
[8] Da Silva L B S, Hellstrom E E and Rodrigues D Jr 2015 The influence of milling time and $ZrB_2$ addition on the superconducting properties of $MgB_2$ *IEEE Trans. Appl. Supercond.* **25** 1–4
[9] Da Silva L B S, Hellstrom E E and Rodrigues D Jr 2014 $MgB_2$ superconductors with addition of $ZrB_2$ and different carbon sources *J. Phys. Conf. Ser.* **507** 012043
[10] Dou S X, Pan A V, Zhou S, Ionescu S, Liu H K and Munroe P R 2002 Substitution-induced pinning in $MgB_2$ superconductor doped with SiC nano-particles *Supercond. Sci. Technol.* **15** 1587
[11] Dou S X, Pan A V, Zhou S, Ionescu M, Wang X L, Horvat J, Liu H K and Munroe P R 2003 Superconductivity, critical current density, and flux pinning in $MgB_{2-x}(SiC)_{x/2}$ superconductor SiC nanoparticle doping *J. Appl. Phys.* **94** 1850–6
[12] Wilke R H T, Bud'ko S L, Canfield P C and Finnemore D K 2004 Systematic effects of carbon doping on the superconducting properties of $Mg(B_{1-x}Cx)_2$ *Phys. Rev. Lett.* **92** 217003
[13] Yamamoto A, Shimoyama J, Ueda S, Iwayama I, Horii S and Kishio K 2005 Effects of $B_4C$ doping on critical current properties of $MgB_2$ superconductor *Supercond. Sci. Technol.* **18** 1323–8
[14] Agatsuma K, Furuse M, Umeda M, Fuchimo S, Lee W J and Hur J M 2006 Properties of $MgB_2$ superconductor by doping impurity of SiC, graphite, $C_{60}$, and C nano-tube *IEEE Trans. Appl. Supercond.* **16** 1407–10
[15] Da Silva L B S, Rodrigues D Jr, Serrano G D, Metzner V C V, Malachevsky M T and Serquis A C 2011 $MgB_2$ superconductors with addition of other diborides and SiC *IEEE Trans. Appl. Supercond.* **21** 2639–42
[16] Da Silva L B S, Vianna A A, Manesco A L R, Hellstrom E E and Rodrigues D Jr 2016 The influence of stearic acid addition on the superconducting properties of $MgB_2$ *IEEE Trans. Appl. Supercond.* **26** 1–4
[17] Rodrigues D Jr, Jiang J, Zhu Y, Voyles P, Larbalestier D C and Hellstrom E E 2009 Flux pinning optimization of $MgB_2$ bulk samples prepared using high-energy ball milling and addition of $TaB_2$ *IEEE Trans. Appl. Supercond.* **19** 2797–801
[18] Rodrigues D Jr, Da Silva L B S, Metzner V C V and Hellstrom E E 2012 Superconducting properties of $MgB_2$ with addition of other $AlB_2$ type diborides and carbon

sources, prepared using high energy ball milling and HIP *Phys. Proc.* **36** 468–74
[19] Dou S X, Soltanian S, Horvat J, Wang X L, Zhou S H, Ionescu M and Liu H K 2002 Enhancement of the critical current density and flux pinning of $MgB_2$ superconductor by nanoparticle SiC doping *Appl. Phys. Lett.* **81** 3419–21
[20] Larbalestier D C *et al* 2001 Strongly linked current flow in polycrystalline forms of the superconductor $MgB_2$ *Nature* **410** 186–9
[21] Rodriguez-Carvajal J 1993 Recent advances in magnetic structure determination by neutron powder diffraction *Physica.* B **192** 55–69
[22] Parisiades P, Liarokapis E, Zhigadlo N D, Katrych S and Karpinski J 2009 Raman investigations of C-, Li- and Mn-doped $MgB_2$ *J. Supercond. Nov. Magn.* **22** 169–72
[23] Serquis A, Liao X Z, Zhu Y T, Coulter J Y, Huang J Y, Willis J O, Peterson D E and Mueller F M 2002 Influence of microstructures and crystalline defects on the superconductivity of $MgB_2$ *J. Appl. Phys.* **92** 351
[24] Sato M and Ishii Y 1989 Simple and approximate expressions of demagnetizing factors of uniformly magnetized rectangular rod and cylinder *J. Appl. Phys.* **66** 983
[25] Bean C P 1962 Magnetization of Hard Superconductors *Phys. Rev. Lett.* **8** 250
[26] Fuchs G, Müller K H, Handstein A, Nenkov K, Narozhnyi V N, Eckert D, Wolf M and Schultz L 2001 Upper critical field and irreversibility line in superconducting $MgB_2$ *Solid State Commun.* **118** 497–501
[27] Dew-Hughes D 1974 Flux pinning mechanism in type II superconductors *Phil. Mag.* B **30** 293
[28] Dew-Hugles D 1987 The role of grain boundaries in determining $J_c$ in high-field high-current superconductors *Phil. Mag.* B **55** 459